International Journal of Plant Science and Ecology
Vol. 6, No. 2, 2020, pp. 14-24
http://www.aiscience.org/journal/ijpse
ISSN: 2381-6996 (Print); ISSN: 2381-7003 (Online)

Forecasting Drought Patterns and Trends in Juba County, South Sudan Using Artificial Neural Networks

David Lomeling*, Salah Joseph Huria

Department of Agricultural Sciences, College of Natural Sciences and Environmental Studies (CNRES), University of Juba, Juba, South Sudan

Abstract

A simple Feed-Forward Neural Network (FFNN) model with a learning back-propagation algorithm was applied to forecast drought patterns derived from rainfall data of Juba County, South Sudan from 1997-2016. The annual rainfall data were aggregated into three seasons MAMJ, JAS and OND and later trained for best predictions for the period 2017-2034 using the Alyuda Forecaster XL software. Best training was attained once the *minimum error* of the weight ΔW and expressed as Mean Square Error between the measured and estimated values. Drought expressed as SPI was derived by fitting the respective CDFs to the rainfall amounts of each season. The results showed that for MAMJ and JAS months, the number forecasts were over 85% whereas this was between 60-80% for OND months. Rainfall forecast showed that the MAMJ months for the years 2019 to 2027 will be moderately wet with near to normal drought except in April 2021 which will experience some severe wetness. Interdecadal severe drought is expected between 2028 to 2033 after almost two decades. Declining trend per decade of SPI for all seasons was significant at $p<0.01$ whereas JAS and OND seasonal decrease in the next 100 years is forecasted to remain within the near to normal range while MAMJ is forecasted to have moderate drought.

Keywords

Feed Forward Neural Network, Drought Forecasting, Cumulative Distribution Function, Training Set, Standard Precipitation Index

Received: March 30, 2020 / Accepted: April 26, 2020 / Published online: June 9, 2020

1. Introduction

A large part of the East African region including South Sudan has over the last twenty years been experiencing significant impacts of climate change. This is noticeable by the erratic spatial-temporal variations of rainfall in both intensity and amounts. Although no prior studies on the seasonality of rainfall distribution in Juba County have been conducted, experiential evidences from farming communities in the region report of clear deviations and decrease below average values especially during the onset of the rainy season (*Ja'be*). Generally, the annual onset rains start during the second to third dekad of April and continues till June punctuated with a dry spell around July. From August, this continues till October significantly decreasing toward November and December dry season (*Méling*). The effects of such temporal shift from the traditional farming calendar could be caused by *El Niño-Southern Oscillation* (ENSO) [1] regimes resulting to untimely availability of soil moisture and consequently into poor harvests or crop failure. Understanding such erratic rainfall events and assessing seasonal rainfall trends would require a differentiated understanding of the effects of "*meteorological drought*" on the "*agricultural drought*". The former is expressed entirely based of the degree of dryness (*usually related to rainfall anomaly from the long-term mean*) whereas the latter is based on temporal soil moisture deficit during crop phenology

* Corresponding author
E-mail address: dr.david_lomeling@gmx.net (D. Lomeling)

coupled with intensive actual evapotranspiration. According to the Intergovernmental Panel on Climate Change (IPCC) AR4 (Fourth Assessment Report), drought may be described as a '*prolonged absence or marked deficiency of precipitation in the topmost one meter of soil layer*`. Much of the rainfall predictions for South Sudan encompassing the study area have in the last decade been issued by diverse regional and international institutions like the IGAD Climate Prediction and Applications Centre, (ICPAC); UN Food and Agriculture Organization (FAO); United Nations Office for the Coordination of Humanitarian Affairs (UNOCHA). These predictions are, however, monthly with short decadal time scales and often in the form of probabilities relative to monthly or seasonal rainfall averages. Often, spatial and temporal rainfall patterns do not correlate with soil moisture contents and dynamics. [2] Showed that surface soil moisture dynamics generally follow rainfall patterns at two gravel plain sites but was not the case in the sand dune site. Therefore, depending on intensity of rainfall, soil structure, surface sealing and infiltration, clear distinctions between meteorological and agricultural droughts should be made and how both are interlinked.

Drought can be measured in absolute terms as a function of precipitation amounts. It can be expressed as; Soil Moisture Deficit Index (SMDI) [3] the Normalized Soil Moisture Index (NSMI) [4] or to more appropriate, the Standardized Precipitation Index (SPI). The Global Climate Observation System (GCOS) program has acknowledged soil moisture as one of the Essential Climate Variable (ESV SM) that will have to be routinely measured and monitored in space and time. In the last three decades, temporal and spatial in-situ soil moisture contents have continuously been measured through satellite-based soil moisture products obtained from active and passive microwave sensors like the Advanced Microwave Scanning Radiometer on Earth Observing System (AMSR-E) [5] or the AQUA AMSR-E [6].

Much research on rainfall prediction using the ANN over the last decades have been conducted in different parts of the world from monthly time series [7]; seasonal [8]; daily [9]; hourly [10]; decadal [11]; monthly [12]. A comprehensive overview of ANNs use in temporal rainfall prediction has been reported by [13]. However, only a few similar studies have been conducted in Africa as in Ethiopia [14]; in Algeria [15] and in West Africa [16].

The main objective of our study was to evaluate the relevance, accuracy and application of FFNN in forecasting seasonal drought patterns derived from historical data.

1.1. ANN Architecture

The ANN model is based on a simplified and popularly used neural network architecture called multilayer perceptron network (MLPN) model (also known as *multilayer feedforward network*) as in Figure 1. Hereby, the product of the values of neurons or impulses $(x_1, x_2, \ldots . x_n)$ from the several input neurons and their respective weighted values $(w_1x_1, w_2x_2, \ldots w_nx_n)$ are passed on to the middle neurons as a sum of $f(w_1x_1, w_2x_2, \ldots w_nx_n)$ or $\sum f(w_ix_i)$ in the hidden layer.

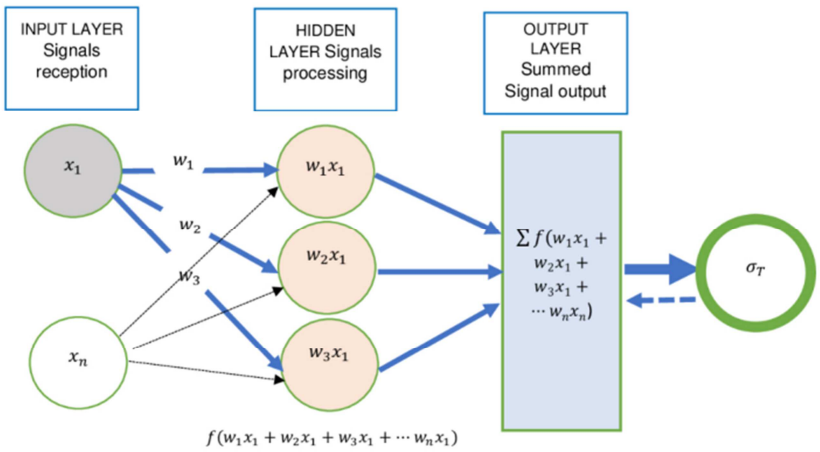

Figure 1. A simple illustration of the FFNN model.

The products from the individual neurons in the hidden layer are passed on upon activation through a non-linear transfer function or *logistic function* $f(x) = \frac{1}{(1+e^f)}$ to produce their respective outputs. The total output of the entire ANN for the specific inputs are compared to the target value (σ_T). The difference is expressed as the measure of error (E) between the computed and expected values. The process of backpropagation from the output to the hidden layer ensues and continues iteratively depending on margin of error till a minimum error value is attained.

1.2. Estimation of SPI

The Standardized Precipitation Index (SPI) is a popularly used index to characterize meteorological drought [17] on varying timescales. SPI is a probability index based entirely on precipitation as input variable. Formulated by [18] it can better represent rainfall anomalies in terms of wetness or drought than for example the Palmer Drought Severity Index (PSDI).

Table 1. Classification scale for the SPI.

Drought		Wetness	
Description	**SPI**	**Description**	**SPI**
Extreme drought	< -2.0	Extreme wetness	>2.0
Severe drought	-1.5 to-2.0	Severely wet	1.5 to 2.0
Moderate drought	-1.0 to -1.5	Moderately wet	1.0 to 1.5
Near normal	-1.0 to 0.0	Near normal	0.0 to 1.0

The first step in calculating the SPI was to determine a Cumulative Distribution Function (CDF) that describes the long-term time series of precipitation observations in either 1, 3, 6-month, etc. intervals. The CDF with mean zero (*corresponds to the median precipitation*), was then applied to the cumulative probability and the SPI estimated. The magnitude of the SPI departure from zero is a probabilistic measure of the severity of a wet or dry event that can be used for risk assessment. Basically, the SPI was envisaged to express the spatial-temporal drought events and variability as influenced by rainfall deficit. It was defined as the number of standard deviations from which normally distributed random variable deviated from its long-term mean. This was obtained by fitting a gamma function $\Gamma(\alpha)$ of the cumulative distribution to precipitation values in the time series (*as in our study a 3-month period*). For most part, the SPI estimates were let to vary between -2.0 and +2.0 which contained approximately 95% of the SPI values with close to 68% within the range -1 to +1.

2. Methodology

This study evaluated the significance of the ANNs in the forecasting of seasonal rainfall patterns in Juba County of Central Equatoria State (CES), South Sudan. In general, there are five basics steps: (1) collecting data, (2) pre-processing data, (3) building the network, (4) training and (5) test performance of model. The basic flow in designing ANNs model is given in Figure 1. The daily rainfall data for Juba weather station as from the years 1983 to 2015 were downloaded from the US National Oceanic and Atmospheric Administration (NOAA). However, daily and consistent rainfall data were only recorded as from 1997 to 2016 and were used for this study. Data pre-processing involved aggregating the daily rainfall amounts to monthly means of March-April-May-June (MAMJ), July-August-September (JAS) and October-November-December (OND). Due to the unpredictable onset of rains especially between mid to end of March of each season, the MAMJ was "*lumped*" together. Rainfall around mid-March prior to the onset of the rainfall season in April was characterized by drizzles and light rainfall showers. With these monthly rainfall data sets, neural networks were then created and later proceeded by training and forecasting. The chosen rainfall data for each season were divided into two random groups, the training and test sets corresponding to 82% and 18% respectively. Networks were trained for a fixed number of epochs or iterations till a minimum error function was reached. The optimal number of neurons in the hidden layer was obtained experimentally running the training process several times until a good performance was obtained or when no other changes were observed.

2.1. Cumulative Distribution Function (CDF) of Gamma Distribution

For some chosen rainfall season and time scale, the CDF $G(x)$ of a gamma distribution (Γ_α) is defined as:

$$G(x) = \frac{1}{\beta^\alpha \Gamma_\alpha} x^{\alpha-1} e^{-\frac{x}{\beta}} \quad (1)$$

where,

$$\Gamma_\alpha = \int_0^\infty e^{-t}\, t^{\alpha-1} dt \quad (2)$$

Where $x > 0$ is the rainfall amount and the gamma distribution parameters $\alpha > 0$ as the shape and $\beta > 0$ the scale parameters and can be estimated through the Maximum Likelihood Estimation (MLE). First, a measure of the skewness (A) with median $m = 0.5$ of all (x_i) non-zero values in the rainfall time series and ($\overline{x_i}$) the arithmetic mean is estimated as:

$$A = \ln(\overline{x_i}) - \frac{\sum_{i=1}^{n} \ln(x_i)}{n} \quad (3)$$

The values for the gamma distribution parameters can then be estimated as:

$$\alpha = \frac{1}{4A}\left(1 + \sqrt{1 + \frac{4A}{3}}\right) \quad (4)$$

$$\beta = \frac{\overline{x_i}}{\alpha} \quad (5)$$

2.2. Data Pre-processing and Training of the Network

In order to enhance a faster convergence to a global minimum, the seasonal rainfall input variables were normalized relative to the total seasonal average. The SPI values were then derived from normalized rainfall values to be consistent with the sigmoid activation function between 0

and 1. Since probability is between 0 and 1, the normalized values would give better predictions during training. The Alyuda ForecasterXL basically splits the data into two sets (1) training set (2) test set. During training, the weights of the neural network are adjusted to increases the accuracy by minimizing the error function (E) during iteration. The training is stopped once the error function reaches a global minimum. Finally, the performance of the network is evaluated on the test data set which had not been involved in the training process. In this study, the neural network was trained with 76, 56 and 55 datasets for the MAMJ, JAS and OND months respectively.

2.3. Model Performance

Model prediction accuracy measured by the error function (E) was tested by both the Mean Standard Error (MSE) and Absolute Error (AE). This is the difference between the observed (x_{ij}) and the predicted ($\hat{x}_{ij}$) for the *i-th* training case at the *j-th* network output and for (n) observations as:

$$\mathrm{AE} = x_{ij} - \hat{x}_{ij} \tag{6}$$

$$\mathrm{MSE} = \frac{1}{n}\sum_{i=1}^{n}\left(x_{ij} - \hat{x}_{ij}\right)^2 \tag{7}$$

In both cases, the error function (E) is directly dependent on the weight component (W) which in turn influences the learning rate (η). This is updated or changed iteratively during gradient descent as:

$$\Delta \mathrm{W} = \eta \frac{\partial \mathrm{E(W)}}{\partial \mathrm{W}} \tag{8}$$

The smaller the error function the better the prediction during the training process. A minimum of five training runs were done on the same data set to obtain the number or iterations that showed the lowest MSE or AE. This was later set as the maximum number of iterations during training and forecasting in the Create network/Options window of ForecasterXL. The performance of the neural network during training is best done by fitting a linear regression coefficient (r^2) of the observed (*actual*) and forecasted data and expressed in terms of good and bad forecasts (*expressed relative to 100% highest accuracy*).

In this study, 76, 56 and 55 data sets for the MAMJ, JAS and OND months respectively were trained with error tolerance for both training and test sets were set at 10 and 30% respectively. For each of the data sets, we started with one input and output layer while adjusting the number of hidden layers between 1 and 3 for best approximation. The training was run several times for each case till the MSE, AE or tolerance error was low and the highest percentage of good forecasts between actual and forecasted data was attained.

3. Results and Discussion

3.1. Neural Network Performance

The trained JAS with smaller dataset (n=56) and single hidden layer appeared to outperform the MAMJ dataset with larger dataset (n=76) and two hidden layers demonstrating the significance of data size. The variances for MAMJ (σ^2=0.252), JAS (σ^2=0.332) and OND (σ^2=0.345) were 0.01, 0.006 and 0.07 respectively. Comparing the variance effects on all datasets, there was a notable difference on learning especially of JAS and OND datasets with similar data size. The MAMJ and OND were characterized by high standard deviation (σ= 0.266) and (σ = 0.1) respectively, whereas for JAS, this was σ = 0.076). However, all training sets achieved statistically significant performances ($r^2 \geq 0.99$) with number of good forecasts over 60%. Figure 2 shows a plot of MSE and AE vs number of iterations during training for the MAMJ, JAS and OND datasets for the years 1997-2015. The error function estimates showed steep gradients prior to 1000-th iteration till convergence at global minima (Figure 3). During training of the MAMJ dataset for example, there was a sharp decrease of the MSE from about 0.016 to as low as 0.0007 while for the AE this was between 0.1 to 0.016. It is seen that both error functions were large at low iteration values decreasing till convergence and subsequently increasing with further iterations.

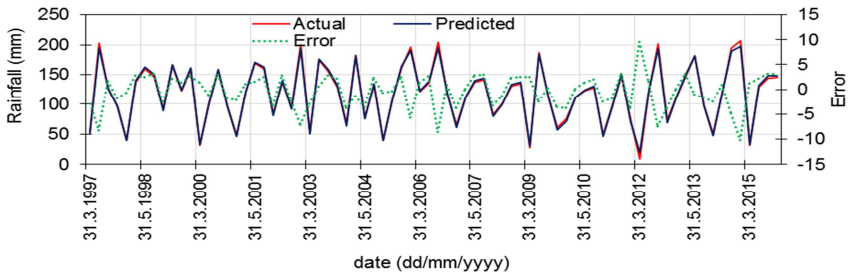

Figure 2. Error estimation between the actual and predicted mean rainfall amounts during training of time series data between 1997 to 2016.

The AE and MSE during training for OND was ten-fold larger that of either MAMJ or JAS. The learning rate (η) measured by number of iterations till global minimum was fastest for OND at 1008 than for JAS or MAMJ at 1625 and

1363 respectively. Low iteration number for OND indicated that the algorithm for stochastic gradient descent effected larger steps with larger errors. This accounted for faster and poor learning rates with poor generalization. Conversely, smaller steps with smaller gradients resulted into larger number of iterations with comparatively lesser errors and better generalization as shown by percentage of good forecasts as in both MAMJ and JAS data sets. The rate of change of the error function ΔW as in Equation (13) therefore, had a significant effect on the performance and accuracy of the ANN.

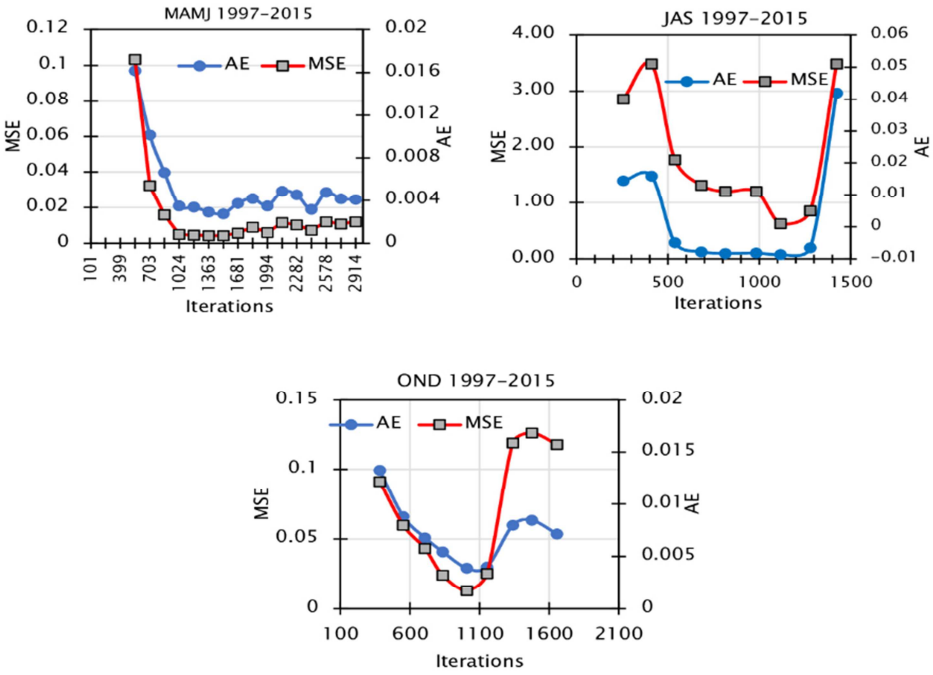

Figure 3. Error development and convergence to global minimum during training of MAMJ, JAS and OND of time series data between 1997 to 2015.

Table 2 shows the training parameters and accuracy according to the r^2, number of good forecasts, hidden layer (s), MSE, and AE. The network demonstrated better performance rate for MAMJ and JAS when using two and one hidden layers respectively. The results here suggest that model performance in terms of the number of good forecasts (98%) was similar for both 1 and 2 hidden layers. In effect, one hidden layer performed just as good as two layers. Similar results on neural performance with a single hidden layer were reported by [19-23]. Although both JAS and OND trained datasets had each one hidden layer and almost equal data size, the latter gave a low number of good forecasts at 61% and high number of bad forecasts (39%). Generally, better accuracy was shown by both MAMJ with 2 hidden layers and JAS only one hidden layer whereas, the OND with 1 hidden layer showed a ten-fold less error margin. In terms of iterations till global minimum, OND data set (1 hidden layer) had the lowest number at 1008, whereas JAS had the highest at 1625 and MAMJ intermediate (2 hidden layers) at 1363. In terms of the percentage of bad forecasts, OND showed the highest inaccuracy. This could be due to the inability to learn from a small dataset, although the learning algorithm for JAS with almost similar data size seemed to work well.

Table 2. Training parameters and network structures showing the goodness of error estimation between the training and test set.

	MAMJ		JAS		OND	
	Training set	**Test set**	**Training set**	**Test set**	**Training set**	**Test set**
Nr. of data set	63	13	47	9	46	9
AE	0.005	0.005	0.003	0.006	0.015	0.02
MSE	4.91E-05	2.35E-05	2.71E-05	7.42E-05	0.0003	0.0004
Error tolerance (%)	10	30	10	30	10	30
Nr. of good forecasts (%)	61 (98%)	13 (100%)	46 (98%)	9 (100%)	28 (61%)	7 (78%)
Nr. of bad forecasts (%)	2 (3%)	0 (0%)	1 (2%)	0 (0%)	18 (39%)	2 (22%)
r^2	0.994		0.996		0.997	
No. of hidden layer (s)	2		1		1	
No. of input layer (s)	1		1		1	
No. of output layer (s)	1		1		1	
Best at iteration number	1363		1625		1008	
Learning rate (η) till global minimum	0.0040		0.0021		0.0062	

Similar observations were reported by [24, 25]. Such conflicting generalizations in terms of the number of hidden layers for MAMJ-JAS as well as for JAS-OND on model performance and accuracy indicate striking instability especially for smaller datasets. For instance, using one hidden layer, the OND dataset had a learning rate of 0.0062 and reached the global minimum at lower iterations than JAS at 0.0021. After that, the error functions AE and MSE started to increase indicating that the model was getting over-fitted.

Moreover, the MAMJ dataset with two hidden layers had a learning rate at 0.004 (Table 2) and was comparatively lower than that of OND but greater than that of JAS dataset with one hidden layer.

Conclusively, one can say, that the learning rate during gradient descent is inversely related to the number of iterations in reaching a global minimum. Judging by the rule-of-thumb in estimating the number of neurons in the hidden layer (s), our study showed that this was between 105 and 210 neurons for one and two hidden layers respectively for MAMJ dataset, whereas these were 99 and 100 neurons for OND and JAS datasets respectively. Despite such striking inconsistency between the JAS and OND datasets with the single hidden layer, the accuracy and generalization performance of the two-layer feed forward neural network model was satisfactory. With the error tolerance (%) as indicator for overall performance, the results demonstrate that, this model was able to achieve remarkable performances on predictive tasks with sufficient data size as in MAMJ and JAS datasets, but unable to perform well on smaller datasets as in OND.

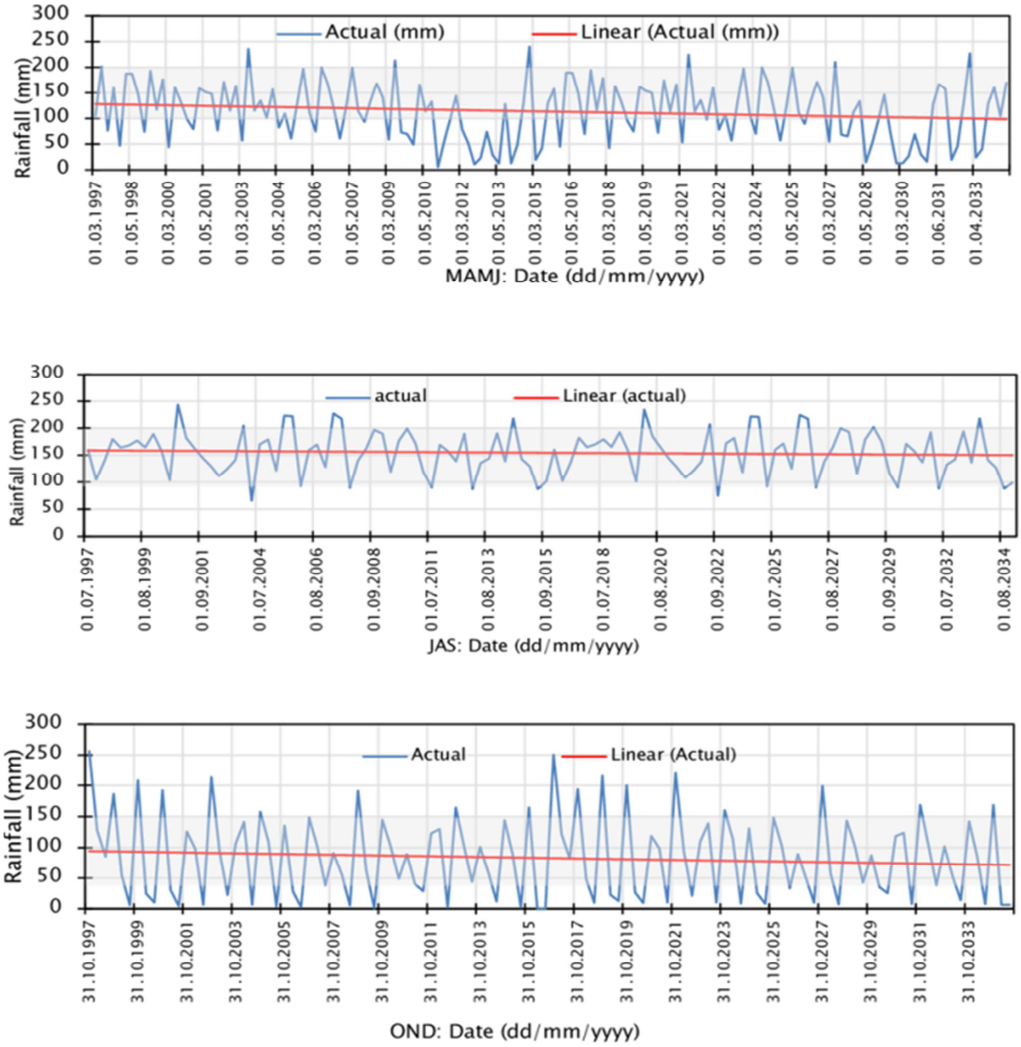

Figure 4. Trendline of rainfall projection between 1997-2034 for the MAMJ, JAS and OND months.

3.2. Inter-seasonal SPI Changes and Drought

The histograms of the SPI during the MAMJ months is shown in Figure 5. It was found that most of the MAMJ months of the preceding years from 1997 to 2016 showed near normal to moderate wetness with similar drought SPI

values. Recurrent severe drought for MAMJ months (red bars) was witnessed during the years 2010-2013 with unusual extreme wetness in July 2014. However, the years 2015 till 2017 showed normal to moderately wet MAMJ months. During 2020, the SPI for the AMJ months are expected to be near normal with moderate drought in March with SPI -0.73, but increase to 1.05 and 0.91 for April and June respectively (Table 3). It is forecasted, that the MAMJ months for the years 2019 to 2027 will be moderately wet with near to normal drought except in April 2021 which will experience some severe wetness (*green bars - due to intensive rainfall*). Interdecadal severe drought at SPI -1.5 to -2.0 with rainfall ranges less than 10th to 5th percentile (< 50 mm) is expected between 2028 to 2033 after almost two decades and is anticipated to have a long duration.

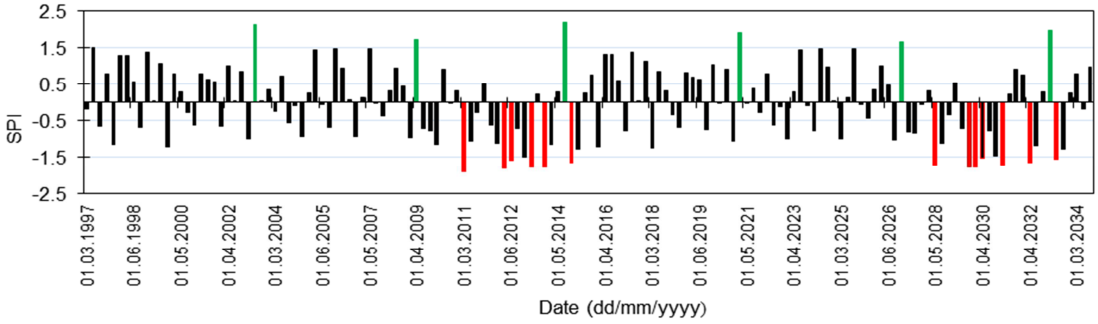

Figure 5. Calculated and projected SPI for the MAMJ months during the period 1997-2034.

For the JAS months, except in 2014, the SPI from 2009-2018 was near normal (Figure 6). In August 2019, moderate drought with SPI -1.3 was followed by sporadic and heavy rainfall ranging between 20th and 10th percentile (about 125 mm). This led to severely wet September month with SPI at 1.96 causing immense flooding in most parts of the county.

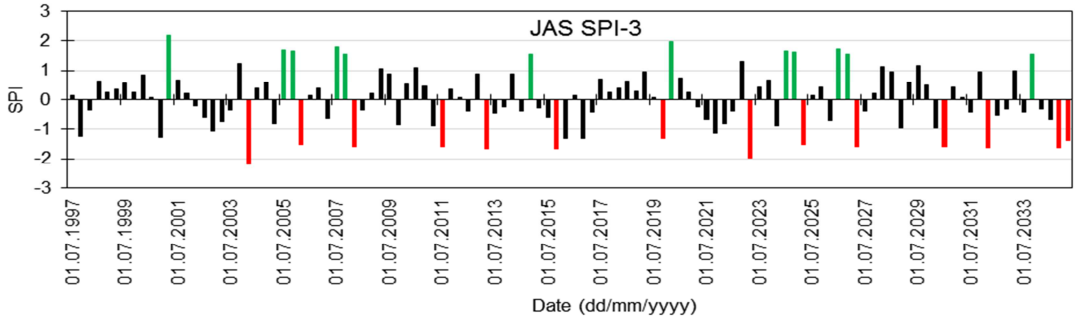

Figure 6. Calculated and projected SPI for the JAS months during the period 1997-2034.

For the MAMJ months (Table 3), five periods of moderate drought between 2021 to 2033 with SPI values between -1.0 and -1.8 at the 40th percentile have been forecasted coupled with periods of severe droughts. Rainfall amounts are expected to vary between 70-90 mm. No extreme droughts have been forecasted during this period. For the JAS months, moderate drought in August 2021 is expected following the generally higher rainfall averages from May to July. For the near future, inter-seasonal severe drought with SPI at -1.9 and a rainfall range between the 10th to 5th percentile has been forecasted for September 2022 (Table 4). Just as in the MAMJ months, no extreme droughts have been forecasted during this period. In our study, we found out that recurrent severe droughts in September are often preceded by severe wetness in July-August and are forecasted to continue till 2034

Table 3. Projected drought periods using SPI values from 2018 to 2034 for the MAMJ Months.

Description	Month/Year
Moderate drought	03/2018, 03/2021, 03/2027, 04/2031, 05/2033
Severe drought	05/2028, 03/2030, 04/2030, 04/2032, 04/2033
Extreme drought	

Table 4. Projected drought periods using SPI values from 2018 to 2034 for the JAS Months.

Description	Month/Year
Moderate drought	08/2021
Severe drought	09/2022, 09/2024, 09/2026, 07/2030, 09/2031, 08/2034
Extreme drought	

For OND months, 2020 is expected to be remain near to normal with moderate drought at SPI -1.0 to -1.5 (rainfall range less than the 20th to 10th percentile) for much of the period except in December which is forecasted to moderately dry (Figure 7). October months have been characterized by severe wetness between 2016-2019 proceeded by moderate drought in November and December months. Moderate drought especially during both months with SPI values between -0.93 to -1.1 respectively and rainfall probability between 10-20% or 20th to 10th percentile is expected to continue till 2027. This moderate drought into the following new MAMJ season may significantly delay the onset of rainfall in March-April. Forecasts till 2034, project that this recurrent phenomenon will ostensibly interrupt the traditional farming-calendar especially during land preparation and sowing.

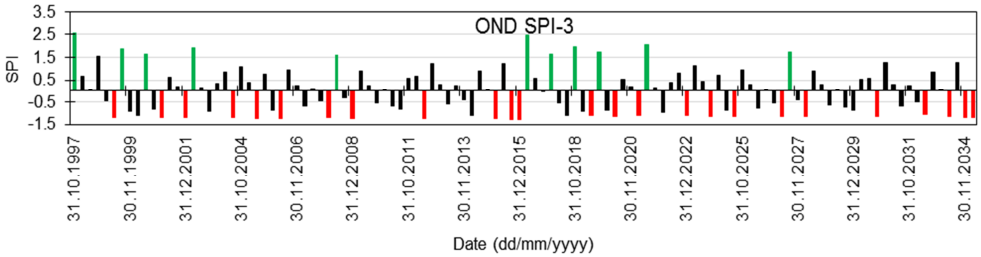

Figure 7. SPI histograms of the different seasons of Juba County.

3.3. Changing Rainfall Patterns and Impacts on Crop Production

Figure 8 shows the anticipated decline in the amount of mean rainfall at the onset of rain during the MAMJ. The onset rains varied between the 4th dekad of February and 1st dekad of March with daily rainfall values generally below 4.0 mm level. The March rainfall amounts locally termed as *´doko kulunyit* (*that which carries away grass cinders after burning*) are barely enough for any effective land preparation and planting. Thus, most farmers tend to shift their land preparation and planting dates toward the 3rd and 4th dekad of April. Most farmers plant cowpeas (*ngete*), amaranth (*kwedekwede*), jute mallow (*mulukhiya/khudra*), okra (*bamia*) whose short growing and maturity periods (from 21 to 70 days) often offers best food security options prior to the onset of the longer rainy JAS season. Increasing inter-seasonal rainfall variability with declining mean rainfall amounts during MAMJ is forecasted to continue, thus much crop production will have to be shifted toward the 4th dekad of April or 1st dekad of May while for maize, sorghum, sesame will have to be grown during the JAS to OND season. Mean onset rainfall amounts in 2018 was expected to be around 65 mm with a 25% probability. With declining amounts of the onset rains, there is need to intensify inter-cropping of fast and slow growing crops during the MAMJ-JAS seasons as much time, energy and water resources can effectively be utilized. These findings corroborate similar studies by [26] on declining rainfall trend in the March-May rains within the East African region.

3.4. Interpretation of the Parameters (α) and (β)

Unlike the normal distribution curve that requires mean, median and mode to define the skewness, the gamma distribution requires that both the shape (α) and scale parameter (β) that are interlinked by Equation (10) be interpreted concurrently. For our study, we varied *a priori* the scale parameter (β) with different values around the mean values to observe the resultant effect on the shape parameter (α).

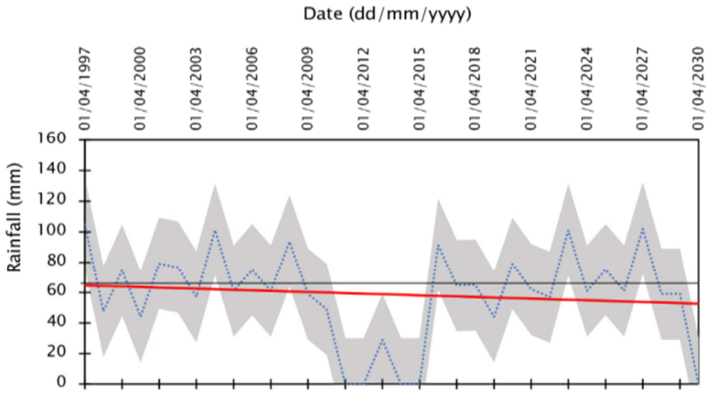

Figure 8. Observed and projected mean rainfall amounts at onset in the first dekad of March (70 days from start of each new year). Black line is the unchanged rainfall means, red line the projected drop.

The scale parameters for MAMJ, JAS and OND months with mean values of 113.32 mm, 154. 6 mm and 84.54 mm were 36.3, 30.6 and 77.3 respectively. We observed that a greater scale parameter (*with correspondingly low shape parameter*) had low mean and variance. Hereby, large scale parameter depicted large variability in rainfall patterns resulting in irregular rainfall typical for the comparatively drier OND months. Conversely, with increasing rainfall during the rainy season (*Ja'be*), the wetter JAS months with high mean and lowest scale parameter (*with correspondingly higher shape parameter*) showed low rainfall variability.

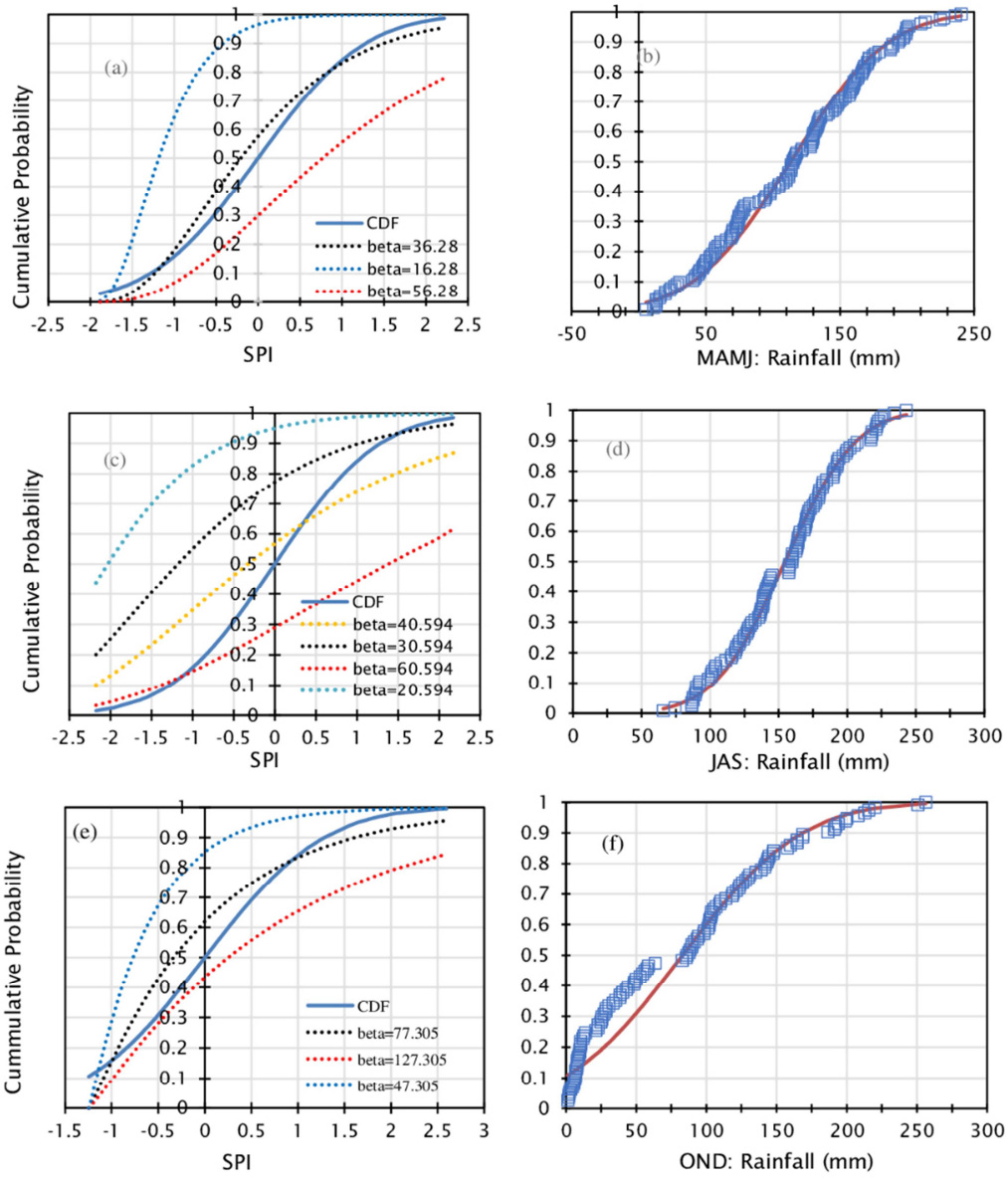

Figure 9. A CDF plot of different shapes of the distribution curves for the three seasons as influenced by different β scale parameters.

The MAMJ months transitioning from the relatively drier OND months showed more, or less similar patterns to the JAS months with intermediate scale parameter and mean (*compared to JAS but higher than OND months*) that was often characterized by occasional rainfall showers in March prior to the onset of the rainy season in April. Hereby, the scale parameter was low with comparatively higher mean suggesting less rainfall variability and therefore wetness. With such interpretation of gamma parameters, it is likely to describe periods of relative wetness or dryness as well as drought-prone times. For example, for the months JAS, the probability for normal wet conditions at SPI=0.5 increased with each scale parameter β as shown in Figure 9 (a). The rainfall probability here at $\beta = 60.594$ is about 0.56, at β =0.594 is about 0.67 and at β =20.594 is about 0.97. To illustrate the interlinkage between scale parameter and rainfall amount at SPI=0.5 constant, a straight line was drawn from Figure 9 (a) that cut the cumulative rainfall in Figure 9

(b). The estimated rainfall amounts at β =60.594, β =30.594 and β = 20.594 were about 140, 168 and 227 mm respectively and showed increasing rainfall amounts with decreasing scale parameter resulting into more negatively skewed CDF. In general, this implies that wetter rainfall conditions have smaller β values than drier conditions. This inverse relationship between scale parameter and rainfall amount may give insight into the rainfall patterns during anytime of the season as in the MAMJ and OND months.

3.5. SPI Future Projections

Though not significant at $p < 0.01$, the observed (1997-2016) and forecasted (2017-2034) SPI for the MMAJ, JAS and OND showed decreasing trends of −0.15, -0.05 and -0.04 respectively. For JAS and OND this decrease in the next 100 years is forecasted to remain within the near to normal range while for MAMJ, is forecasted to have moderate drought. The reason is the low mean rainfall during OND coupled with high daily temperatures around this period that often continues into the MAMJ months prior to the onset of the first rainfall. Manufacturing industries and large-scale agricultural farming that generate large CO_2 or methane emissions are practically non-existent within Juba County and therefore, such "*anthropogenic compulsions*" are unlikely to be the causes for local weather changes influencing rainfall patterns. However, increased burning of fossil fuel, indiscriminate cutting down of forest trees as cheap energy source [27] over the last 50 years may suggest a possible anthropogenic cause for the prolonged heatwave events from hot and dry months, as less CO_2 is being sequestered. Deforestation within a given domain is known to affect local hydrological cycle or regime through reduced evapotranspiration, ET and so increase the likelihood for drought occurrence.

However, effects of global warming exacerbated by El Niño Southern Oscillation on rainfall patterns at the regional level may have occurred, but this could not be statistically identified and verified within the available historical rainfall data.

4. Conclusion

Time series rainfall data from 1997 to 2015 were trained, tested and used to make 3-months forecast. The performance of the ANNs model based on the AE and MSE, degree of tolerance as well as the number of good forecasts during training and testing indicated that the ANN model was accurate enough in forecasting seasonal rainfall. Rainfall projection to year 2034 showed that there was negative monotonic trend ($p<0.01$) for all seasons with amounts varying between 5-12% below seasonal averages. There was also decreasing trend in the average rainfall amounts during onset with much rainfall events occurring towards the end 3rd and 4th dekad of April and in other instances in the 1st dekad of May of each year significantly affecting the timing for land preparation and subsequently planting. Given the projected SPI, three El Niño Southern Oscillation regimes have been projected between 2018 and 2027 for the MAMJ months increasing the probability for poor rain onset. National, state governments as well as development partners will be urged to prepare contingency and intervention plans that could quickly and timely be implemented to avert any disruptions on crop production. Inherent challenges on the application of ANN models in projecting spatial and temporal rainfall patterns, especially on shorter hourly and daily time scales persist. Understanding rainfall variability and intensity on hourly and daily basis within Juba County would increase the capacities and readiness of all stakeholders to timely and adequately respond to uncertainties arising from erratic rainfall patterns and drought. This paper recommends further studies to investigate whether such seasonal projections of rainfall can be corroborated with empirically measured rainfall amounts from several spatially placed stations within the county.

Declaration of Conflicting Interests

The authors declared no potential conflicts of interest with respect to the research, authorship, and/or publication of this article.

Funding

The authors disclose that no financial support for authorship nor publication of this article was received from any institution or body.

Acknowledgements

We thank the US National Oceanic and Atmospheric Administration (NOAA) for enabling us access weather data on Juba, South Sudan from its servers.

References

[1] Fer, I., Tietjen, B., Jeltsch, F. and Wolff, C. (2017). The influence of El Niño–Southern Oscillation regimes on eastern African vegetation and its future implications under the RCP8.5 warming scenario. Biogeosciences, 14, 4355–4374. https://doi.org/10.5194/bg-14-4355-2017.

[2] Li, B., Wang, L., Kaseke, K. F., Li, L., Seely, M. K. (2016). The Impact of Rainfall on Soil Moisture Dynamics in a Foggy Desert. PLoS ONE 11 (10) e0164982. doi: 10.1371/journal.pone.0164982.

[3] Narasimhan, B., Srinivasan, R. (2005). Development and evaluation of Soil Moisture Deficit Index (SMDI) and Evapotranspiration Deficit Index (ETDI) for agricultural drought monitoring. Agric. For. Meteorol. 133, 69–88.

[4] Dutra, E., Viterbo, P. and Miranda P. M. A. (2008). Era-40 reanalysis hydrological applications in the characterization of regional drought Geophys. Res. Lett. 35, L19402.

[5] Njoku, E., Jackson, T., Lakshmi, V., Chan, T., Nghiem, S. (2003). Soil moisture retrieval from AMSR-E, IEEE Geosc. Remote Sens. Let. 41 (2), 215–229. doi: 10.1109/TGRS.2002.808243.

[6] Owe, M., de Jeu, R., Holmes, T. (2008). Multi-sensor historical climatology of satellite-derived global land surface moisture, J. Geophys. Res., 113 F01002, doi: 10.1029/2007JF000769.

[7] Abbot, J. and Marohasy, J. (2017a). Forecasting extreme monthly rainfall events in regions of Queensland, Australia using artificial neural networks. Int. J. Sustain. Dev. Plan. 12 (7), 1117–1131.

[8] Hartmann H, Snow JA, Su B (2016) Seasonal predictions of precipitation in the Aksu-Tarim River basin for improved water resources management. Glob. Planet. Chang. 147: 86–96.

[9] Devi, S. R. P., Arulmozhiyarman, C., Venktash, C. and Pramay, A. (2016). Performance comparison of artificial neural network models for daily rainfall prediction. International Journal of Automation and Computing, 13 (5), 417-427.

[10] Hung, N. Q, Babel, M. S, Weesakul, S. and Tripathi, N. K. (2009). An artificial neural network model for rainfall forecasting in Bangkok Thailand Hydrol. Earth Syst. Sci. 13, 1413–1425.

[11] Warsito, B., Gernowo, R., Sugiharto, A. 2016. Rainfall prediction by using wavelet general regression neural network. Int. J. Appl. Math. Stat. 54 (3), 32–41.

[12] Haviluddin, M., Hardwinarto, S., Sumaryono, M. A. (2015). Rainfall Monthly Prediction Based on Artificial Neural Network: A Case Study in Tenggarong Station, East Kalimantan -Indonesia Procedia Computer Science 59, 142 – 151.

[13] Abbot, J. and Marohasy, J. (2017b). Skillful rainfall forecasts from artificial neural networks with long duration series and single month optimization. Atmospheric Research 197, 289-299.

[14] Elsanabary, M. H. and Gan, T. Y. (2014). Wavelet analysis of seasonal rainfall variability of the Upper Blue Nile Basin, its teleconnection to global sea surface temperature, and its forecasting by an artificial neural network. Mon. Weather Rev., 142, 1771–1791.

[15] Benmahdjoub, K., Amour, Z. and Boulifa, M.- (2013). Forecasting of rainfall using time delay neural network in Tizi-Ouzou (Algeria). Terra-green 13 international conference 2013- advancements in renewable energy and clean environment Energy Procedia 36, 1138–1146.

[16] Badr, H. S., Zaitchik, B. F. and Guikema, S. D. (2014). Application of statistical models to the prediction of seasonal rainfall anomalies over the Sahel. J. Appl. Meteorol. Climatol. 53 (3), 614–636.

[17] Hayes, M., Svoboda, M., Wall, N. and Widhalm, M. (2011). The Lincoln Declaration on Drought Indices: Universal Meteorological Drought Index Recommended. Bull. Amer. Meteor. Soc. 92, 485–488. doi: http://dx.doi.org/10.1175/2010BAMS3103.1.

[18] McKee, T. B., Doesken, N. J. and Kleist, J. (1993). The Relationship of Drought Frequency and Duration to Time Scales. Eighth Conference on Applied Climatology, 17-22 January 1993, Anaheim, California.

[19] Christiansen, N. H, Voie, N. H., Winther, P. E. T., Høgsberg, O. J. (2014). Comparison of Neural Network Error Measures for Simulation of Slender Marine Structures, Journal of Applied Mathematics, Article ID 759834, 11 pp. http://dx.doi.org/10.1155/2014/759834.

[20] Nakama T. Comparisons of Single- and Multiple Hidden-Layer Neural Networks. In: Liu D, Zhang H, Polycarpou M, Alippi C, He H. (eds) Advances in Neural Networks – ISNN 2011. ISNN 2011. Lecture Notes in Computer Science, vol 6675. Springer, Berlin, Heidelberg.

[21] Sonntag, E. D. (1992). Feedback stabilization using two-hidden-layer nets. IEEE Transactions on Neural Networks 3, 981–990.

[22] Lolli, F., Gamberini, R., Regattieri, A., Balugani, E., Gatos, T., Gucc, S. 2016. Single-hidden layer neural networksfor forecasting intermittent demands. International Journal of Production Economics 183 (A), (116-128). https://doi.org/10.1016/j.ijpe.2016.10.021.

[23] Mahmoud, O., Anwar, O., Jimoh F. E. S. M. 2007. Learning Algorithm Effect on Multilayer Feed Forward Artificial Neural Network Performance in Image Coding. Journal of Engineering Science and Technology, 2 (2), 188–199.

[24] Shaikhina, T., Khovanova, N. A. 2017. Handling limited datasets with neural networks in medical applications: A small-data approach. Artificial Intelligence in Medicine, 75, 51-63. http://dx.doi.org/10.1016/j.artmed.2016.12.003.

[25] Forman, G., Cohen, I. 2004. Learning from little: comparison of classifiers given little training. Proc. PKDD 19, 161–72.

[26] Rowell, D, P., Booth, B. B. B., Nicholson, S. E., Good, P. 2015. Reconciling past and future rainfall trends over East Africa. J. Climate, 28, 9768–9788. https://doi.org/10.1175/JCLI-D-15-0140.1.

[27] Lomeling, D., Modi, A. L., Moti, S. K., Kenyi, M. C., Silvestro, G. M., Yieb, J. L. L. (2016). Comparing the Macro-aggregate Stability of Two Tropical Soils: Clay Soil (Eutric vertisol) and Sandy Loam Soil (Eutric leptosol). International Journal of Agriculture and Forestry, 6 (4): 142-151.